Multiband Metasurface-Based Absorber for Applications in X, Ku and K Bands

H. J. S. Coelho[1], B. Araújo[2], M. W. B. Silva[1], T. N. Ferreira[1], A. L. P. S. Campos[3], C. Junqueira[4], Erich Kemptner[5]and Andrey Osipov[5]

[1]Telecommunications Engineering Department, Fluminense Federal University, Niterói, Brazil
[2]TELECOM-EMA, ENAC, Toulouse 31055, France and ISAE-SUPAERO, Toulouse 31055, France
[3]Communication Engineering Department, Federal University of Rio Grande do Norte, Natal, Brazil
[4]Espectro LTDA, Campinas, 13084-012, Brazil, and Department of Communications, Faculty of Electrical and Computer Engineering, University of Campinas, Campinas, 13083-852, Brazil.
[5]Microwaves and Radar Institute, German Aerospace Center (DLR), 82234 Wessling, Germany.

Key Points:

- Metamaterial
- Absorber
- Multi-band
- Metasurface

Corresponding author: M. W. B. Silva, `mauriciobenjo@id.uff.br`

Abstract

In this paper, a slotted-circle patch metasurface that can efficiently absorb electromagnetic (EM) waves in three different bands is proposed. Based on the fundamental resonance of a single circular patch, EM resonances are generated making slits in the circular patch leading to multi-band operation. Simulation results show that the proposed structure can absorb signals in three different bands, namely at 8.10 GHz, 15.39 GHz, and 19.7 GHz with absorption peaks of 99.8%, 99.7%, and 99.8%, and absorption bandwidths of 132 MHz, 181 MHz and 90 MHz, respectively. The absorption mechanism is discussed on the basis of the single-layer effective medium (SLEM) model and the analysis of surface current and electric field distributions. Furthermore, the experimental results show good agreement with the numerical simulations, with an average absorption greater than 99%. The 2-mm thick absorber is electrically thin, corresponding to $\sim \lambda/18$ at its lowest operating frequency. Compared to other published designs, the proposed absorber has a single resonator with simple geometry, but operates in multiband. Therefore, it can be used in many applications such as anechoic chambers, scattering control, photodetectors, microbolometers, and solar cells. **The proposed metasurface absorber can be used for microwave energy harvesting as well as sensor and RCS reduction applications.**

1 Introduction

Manipulation of electromagnetic (EM) waves is desirable for many reasons, such as controlling of the polarization states, providing Electromagnetic Interference (EMI) Shielding, absorption, and radar cross-section (RCS) reduction, to name a few (Karamirad et al., 2020; Ängskog et al., 2018; Ford & Chambers, 2007; Pang et al., 2020). EM wave absorption measures the ability of a structure to attenuate incoming waves (Knott et al., 2004). Conventional absorbers are mainly designed using gradual impedance matching techniques for broadband absorbers, or through resonant techniques, which generally require a metal plate placed a quarter wavelength away from a load to achieve free-space impedance matching. However, both approaches can have practical limitations due to their bulky configurations (Zadeh & Karlsson, 2009; Gau et al., 1997).

The metasurface is a sort of two-dimensional metamaterial structure, whose thickness and periodicity are small when compared to the operating wavelength (Padooru et al., 2012; Holloway et al., 2009). Therefore, both the thickness and periodicity can be used to develop miniaturized structures, as well as to manipulate EM waves, including absorption (Cong et al., 2015; S. Wang et al., 2019; Lim & Lim, 2019). Some perfect absorbers based on the concepts of metamaterials have been proposed for frequencies ranging from microwave to optics (Ghosh & Srivastava, 2017; H. Li et al., 2011; Agarwal & Meshram, 2018; Zhao et al., 2019; Huang et al., 2018; B.-X. Wang et al., 2019; Pan et al., 2021). Metamaterial-based absorbers can work single-band, multiband, and broadband, and they can even switch the frequency absorption effects. In practice, to obtain such functionality, some of these absorption devices use multilayer designs to obtain more absorption bands, which limit their practical applications. To overcome this limitation, many studies have proposed the development of new devices that combine multiple resonant structures into a single unit cell. In this case, the authors consider the fact that resonators with different sizes resonate at different frequencies, obtaining multiple absorption peaks along the electromagnetic spectrum. As an example, a metasurface-based multiband terahertz absorber was designed by combining four different square split-ring resonators into a unit cell (X. Wang et al., 2017). Islam *et al.* proposed a penta-band EM absorber consisting of different combined elements, which can work in different bands in the microwave regime (Islam et al., 2021). However, the disadvantage of this method is that it is difficult to fit different sizes of arrays in the same plane. In addition, unit cells with resonators of different sizes can lead to non-homogeneous characteristics due to the large cell sizes (H. Li et al., 2011; Luo et al., 2011). Although other studies have

proposed multiband absorbers, they have either complex structures or weak absorption peaks (Chaurasiya et al., 2015; Yang & Xia, 2020; Sarkhel & Chaudhuri, 2017).

This work proposes a multiband ultrathin metasurface-based absorber with high-angle stability and polarization insensitivity in X-, Ku-, and K-bands. We show that a unit cell composed of a single resonator, which is a simple circular patch with slits, can generate multiple absorption bands. Both the numerical and the experimental results show that resonances occur at 8.36 GHz, 8.78 GHz, 13.44 GHz, 15.56 GHz, and 19.42 GHz with absorption peaks of 95.4%, 99.7%, 97.5%, 97.3%, and 99.8%, respectively. The absorber is electrically thin with 2 mm of thickness, corresponding to $\sim \lambda_0/18$ at its lowest operating frequency.

2 Proposed Design

The unit cell of the proposed absorber is composed by a circular patch with slits at the top of a grounded FR-4, with $\varepsilon_r = 4.3$, $\tan\delta = 0.02$ and thickness h of 2 mm, Fig. 1. By adjusting the number of slits and their width and length, plasmonic resonances are generated by the electrical and magnetic responses of the circle-shaped geometry, and, thus, the number of absorption peaks, as well as their locations, can be controlled. Moreover, the upper and lower layers are made from a copper film with a thickness of 35 μm and electrical conductivity $\sigma = 5.8 \times 10^7$ S/m. The geometrical parameters, shown in Fig. 1(b), are set to be, in mm, $l_1 = 5$, $l_2 = 5.4$, $l_3 = 5.8$, $d = 0.2$, $g = 0.1$, $R = 6.62$, and $P = 13.24$.

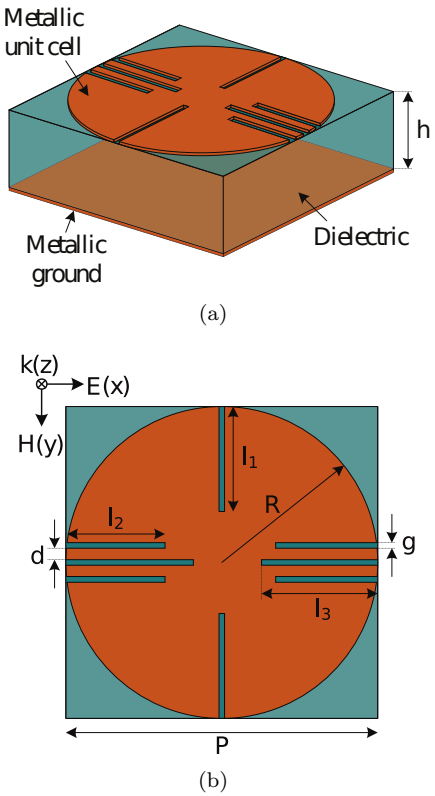

Figure 1. Perspective (a) and top (b) views of the unit cell of the proposed absorber.

Based on the configuration explained above, two important issues regarding the design should be addressed. The first one is related to the choice of a proper dielectric sub-

strate and its thickness, since the dielectric must have sufficient space for an incident wave to remain within the structure and to be absorbed. Moreover, simple slotted circular-shaped plasmonic metasurfaces provide multiple resonances due to their surface current distribution (Bhattacharyya et al., 2013). The fulfillment of this requirement ensures that the incident electromagnetic wave can be reflected from the ground plane and properly absorbed inside this structure. With the optimized structure parameters of the slotted circular-shaped resonator, it is possible to tune the resonant frequencies, resulting in multiple absorption peaks.

Ansys HFSS is used here to carry out simulations. In the simulation setup, a single unit cell with periodical boundary conditions along the x- and y-directions is used to emulate an infinite periodic structure. In addition, to validate the proposed structure, a prototype is manufactured with dimensions of 25 cm $\times$ 25 cm $\times$ 2 cm, Fig. 2.

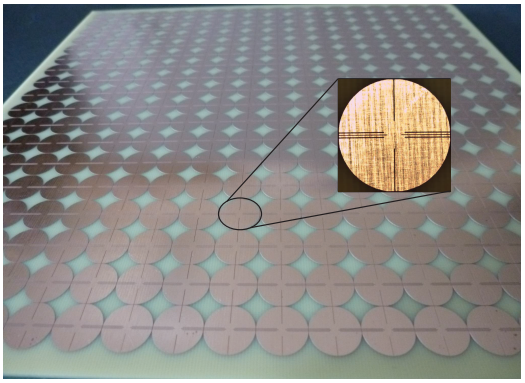

Figure 2. Prototype of the proposed multiband absorber.

3 Theoretical and Numerical Analysis

The working principle of the proposed absorber can be understood by considering its absorptivity rate $A(\omega)$, which is given by the relation between the reflectance $R(\omega)$ and transmittance $T(\omega)$:

$$A(\omega) = 1 - R(\omega) - T(\omega) = 1 - |S_{11}|^2 - |S_{21}|^2. \tag{1}$$

According to Eq. 1, the absorptivity rate is maximized when both transmission and reflection have minimum values at the same time. For an absorber, the transmission can be ignored due to a metallic layer on the backside of the substrate ($T(\omega) = |S_{21}|^2 = 0$), as shown in Fig. 1. Therefore, the absorptivity can be expressed by $A(\omega) = 1 - R(\omega) = 1 - |S_{11}|^2$. Although the proposed unit cell has almost isotropic geometry, the reflected EM wave include the co- and cross-polarized reflection components (Faniayeu et al., 2020; S. J. Li et al., 2020), which can be quantified as follows:

$$R(\omega) = |S_{11}|^2 = |R_{xx}|^2 + |R_{yx}|^2 = |S_{11,xx}|^2 + |S_{11,yx}|^2, \tag{2}$$

where the co- and cross-polarized components are represented by xx and yx, respectively. Therefore, the absorption can be calculated by

$$A(\omega) = 1 - R(\omega) = 1 - |S_{11,xx}|^2 - |S_{11,yx}|^2. \tag{3}$$

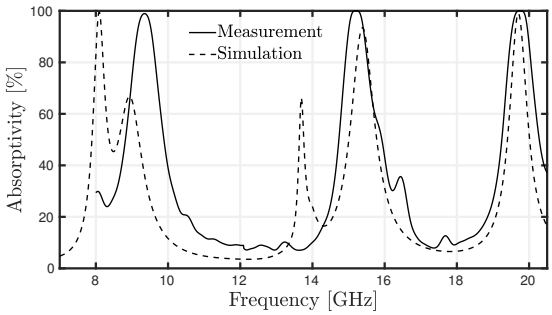

Figure 3. Simulated and measured absorptivity of the proposed structure.

The effective constitutive parameters of the unit cell can be calculated from the $S-$parameters as well, providing an important insight into the mechanism of absorption of the proposed design. Thus, the effective relative permittivity ε_{eff} and permeability μ_{eff} can be expressed as (Bhattacharyya & Srivastava, 2014)

$$\varepsilon_{eff} = 1 + \frac{2j}{k_0 h}\left(\frac{1 - S_{11}}{1 + S_{11}}\right), \tag{4}$$

$$\mu_{eff} = 1 + \frac{2j}{k_0 h}\left(\frac{1 + S_{11}}{1 - S_{11}}\right), \tag{5}$$

where k_0 is the free-space wavenumber, S_{11} is the reflection coefficient under normal incidence, and h is the thickness of the substrate. Also, the input impedance Z_{in} of the absorber can be written as

$$Z_{in} = \sqrt{\frac{\mu_{eff}}{\varepsilon_{eff}}}. \tag{6}$$

When the Z_{in} is equal to the free-space impedance Z_0, there will be no reflection of the incident EM wave and, thus, the absorptivity will be at its maximum.

4 Results and Discussion

Considering Eq. 3, the absorptivity of the proposed absorber under normal incidence was calculated, as can be seen in Fig. 3. For the simulated absorptivity, one can note three main absorption peaks at 8.10 GHz, 15.39 GHz, and 19.7 GHz, along with maximum levels of absorption of 99.43%, 93.45%, and 99.02%, with bandwidths of 132 MHz, 181 MHz and 90 MHz, respectively. For the measured results, the maximum absorption happens at 9.35 GHz, 15.21 GHz, and 19.76 GHz with maximum values of 98.94%, 99.99%, and 99.99%, respectively. Comparing both results, there is a frequency shift only at lowest-frequency absorption, which is due to the manufacturing tolerances, while the results are well-matched at the upper bands.

4.1 Measurements

The experimental characterization of the proposed 18 x 18 array, shown in Fig. 2, was carried out in an anechoic chamber of the German Aerospace Center (DLR) laboratories using the free space method, as shown in Fig. 4. For this purpose, three pairs of conical horn antennas (operating in X, Ku and K band), connected to a Vector Network Analyzer (Anritsu VNA MS4644B), have been used in the experiment. Dielectric lenses have been used to transform spherical waves to plane waves.

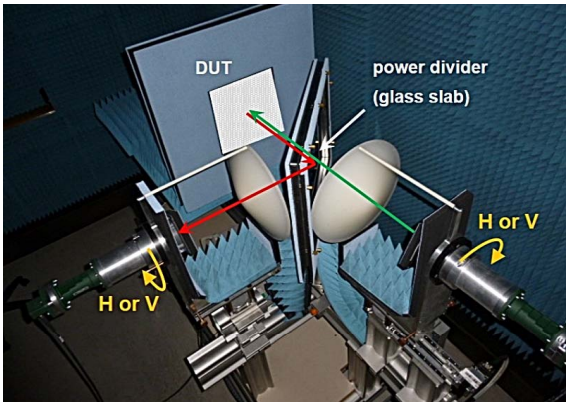

Figure 4. Photograph of the proposed metamaterial absorber measurement procedure.

Furthermore, a power divider, a flat glass plate, is inserted between the transmitting antenna and the sample and twisted by 45°, as shown in the Fig. 4. A second antenna was mounted for the reflected path of the wave. Both antennas can be rotated independently by 90° in order to enable H as well as V polarization. Thereby full polarimetric reflection measurements can be executed.

The thickness of the glass plate is optimized to divide the energy of the incident wave in such a way that both the transmitted and the reflected wave are attenuated by approximately 3 dB in the case of normal incidence. This is only possible by applying different glass plates for each frequency band. The thicknesses are 3 mm (X band), 2 mm (Ku band) and 1.35 mm (K band). These values are only valid for the given quality of glass ($\varepsilon_r^{'} = 6.8$, $\varepsilon_r^{''} = 0.08$). In the case of 45° incidence, the attenuation values are approximately 5 dB (transmission and TE polarization; reflection and TM polarization) and 1.5 dB (transmission and TM polarization; reflection and TE polarization).

An advantage of this measurement technique is the increase of the signal dynamics for co-polar reflection measurements. They could also be performed by a simple VNA-S11 measurement without the glass plate and without the second antenna. But in this case the signal dynamics is decreased by the internal directional coupler of the VNA.

In the case of co-polarization, the reflection measurements were normalized against the reflection response of a flat metal plate having the same size as the absorber sample. With cross-polar measurements, in contrast to co-polar measurements, it is not possible to normalize such measurements using a flat metal plate; the attenuation values of the glass plate are used instead.

Finally, to obtain the absorption values of the investigated sample (see Eq. 2) the determined co- and cross-polarized reflection data of the absorber is deducted from the measured reference data.

4.2 Mechanism of Absorption

To understand the mechanism of absorption of the proposed design, the single-layer effective medium (SLEM) model is employed, which is often used in the literature (Watts et al., 2012; Landy et al., 2008; Tao et al., 2008). In this work, the proposed absorber consists of three layers: a metal circular patch, a dielectric substrate, and a metal ground plane. However, by employing the SLEM model, this absorber can be understood as a single layer of a homogeneous medium, which is characterized by its effective relative permittivity ε_{eff}, permeability μ_{eff} and normalized input impedance Z_{eff}.

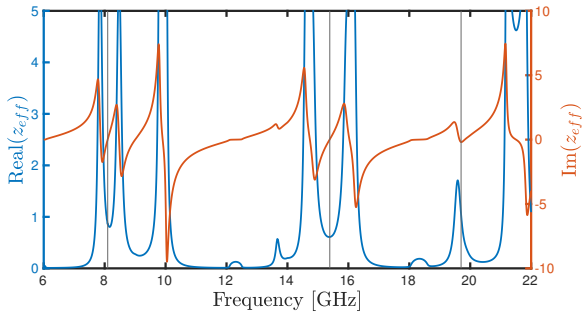

Figure 5. Real and imaginary parts of the normalized impedance of the proposed structure.

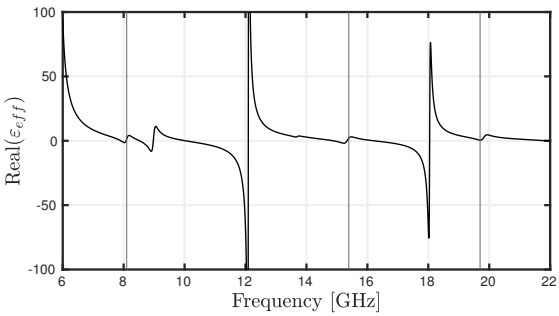

(a)

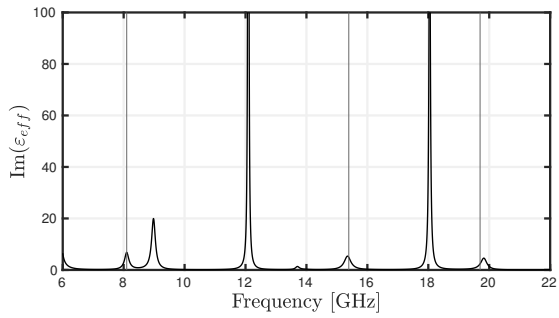

(b)

Figure 6. Real (a) and imaginary (b) parts of the effective permittivity of the proposed structure.

Figure 5 presents the simulated normalized input impedance Z_{eff}. One can note that the real part of Z_{eff} is close to unity, and the imaginary part is close to zero for all three absorption peaks, which leads to minimum reflection and maximum absorptivity (see Eq. 1). This is due to the fact that the reflection coefficient can be written as $\Gamma = (Z_{eff} - 1)/(Z_{eff} + 1)$. Furthermore, Table 1 presents the values of the real and imaginary parts of the impedance of the metamaterial absorber (MMA) at 8.10 GHz, 15.39 GHz, and 19.70 GHz, which were retrieved by using the SLEM model, as well as the effective permittivity and permeability, which are discussed next.

Figures 6 and 7 show the simulated effective permittivity and permeability of the proposed absorber, respectively. Around 8.1 GHz and 15.39 GHz, an electric response is observed with the variation of the real part of ε_{eff} from negative to positive values,

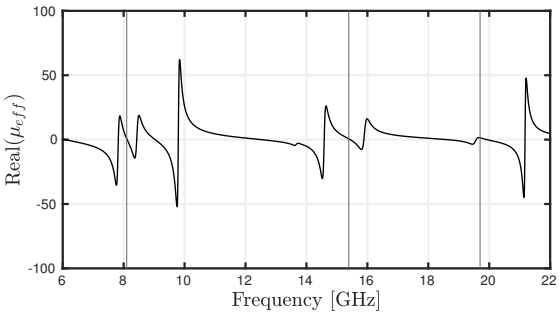

(a)

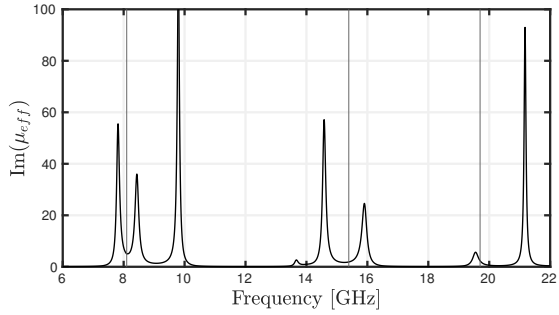

(b)

Figure 7. Real (a) and imaginary (b) parts of the effective permeability of the proposed structure.

Table 1. Retrieved constitutive electromagnetic parameters of the proposed metasurface absorber.

Frequency	Real Part			Imaginary Part		
[GHz]	ε_{eff}	μ_{eff}	Z_{eff}	ε_{eff}	μ_{eff}	Z_{eff}
8.10	1.358	0.730	0.864	6.776	5.107	0.024
15.39	2.016	0.610	0.612	4.897	1.882	-0.009
19.7	0.516	1.474	0.965	2.393	2.356	-0.189

and the same behavior for the same frequencies is noted for the real part of μ_{eff}, and, then, the high absorption observed at these frequencies is due to both electric and magnetic responses. On the other hand, at 19.7 GHz, no electric response is observed from Re(ε_{eff}) and only a magnetic one can be noted, thus, the absorption at this frequency is mainly driven by the magnetic response.

The absorption mechanism can be understood as well through the analysis of the surface current density distribution on the top and bottom metal layers of the proposed MMA for the different absorption peaks, which is shown in Fig. 8 considering an incoming electromagnetic wave under normal incidence with an x-directed electric field. One can note that there is a surface current concentration at the upper and lower edges of the circle-shaped top layer as well as in the vertical slits. The analysis of the surface current distribution allows an insight into the principles of wave absorption of the proposed structure. Moreover, when compared to the top layer, the intensity of the surface current on the ground plane is weaker because the intensity of the incident wave decays as

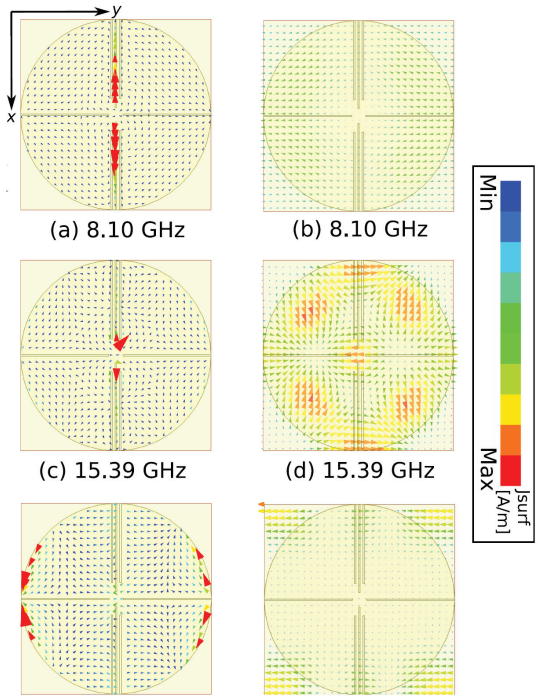

Figure 8. Surface current distribution on the top (a, c, e) and ground plane (b, d, e).

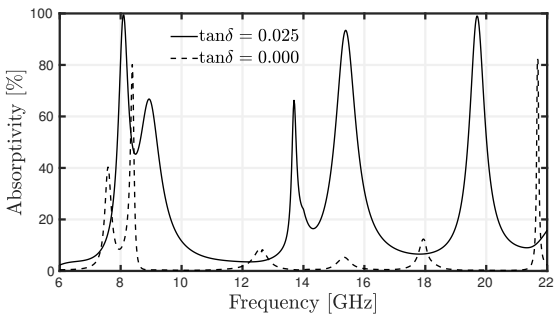

Figure 9. Simulated absorptivity of the proposed structure for a dielectric substrate, where the loss tangent tanδ is equal to 0.025 and 0.000.

it travels through the MMA. Furthermore, the circle-shaped structure responds to the incident EM wave by generating anti-parallel currents between the top geometry and ground plane, which results in current circulation perpendicular to the magnetic field applied within the MMA that excites a magnetic dipole.

When it comes to absorbers, it is important to understand the influence of their main components on the absorption of the incident electromagnetic wave. To this end, the absorptivity of the proposed structure is calculated considering both a lossless (tanδ = 0.000) and lossy FR-4 substrate (tanδ = 0.025), see Fig. 9. One can note that the absorption happens inside the substrate, once the level of absorptivity is low, *i.e.* below 40%, for the lossless substrate at the three main frequencies of absorption, namely 8.10 GHz, 15.39 GHz, and 19.7 GHz. Therefore, it is possible to point out that almost all energy is absorbed inside the loss substrate, and that the loss tangent of the FR-4 plays an important role in it.

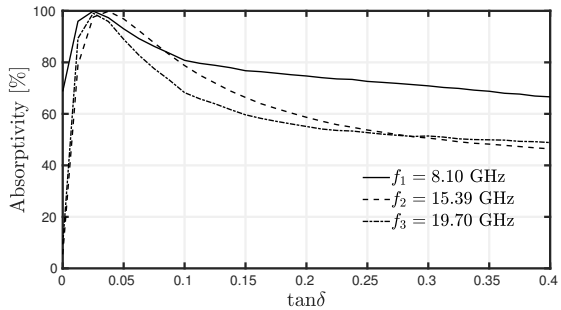

Figure 10. Absorptivity as a function of the tangent loss of the substrate.

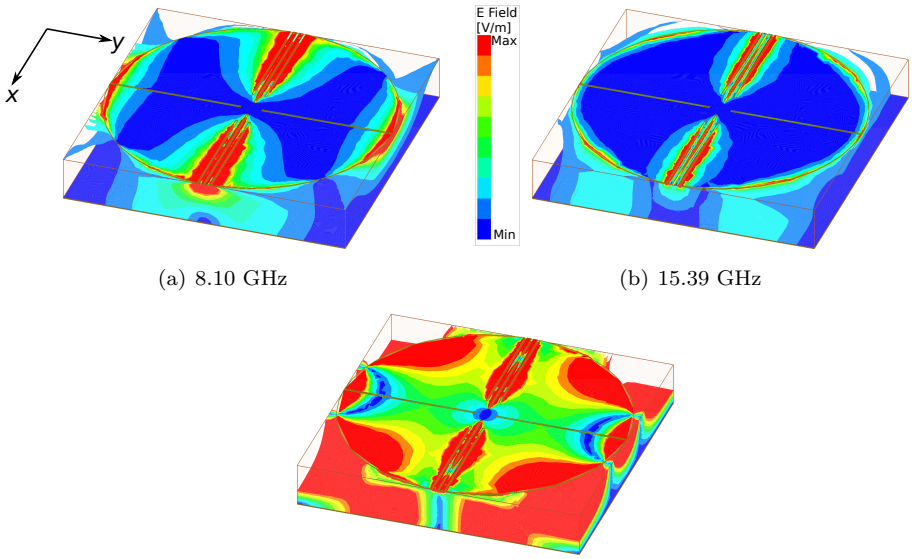

(a) 8.10 GHz (b) 15.39 GHz

(c) 19.70 GHz

Figure 11. Electric field distribution on the proposed absorber.

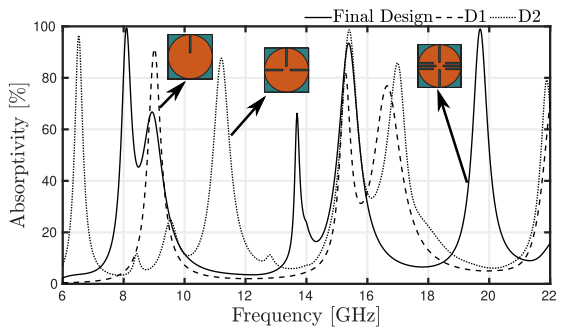

Figure 12. Absorptivity of the proposed absorber for different design stages.

As it was observed, most of the incident wave is absorbed inside the substrate. To provide good insight into it, Fig. 10 shows the performance of the proposed absorber as a function of the loss tangent of the substrate. From $\tan\delta = 0$, the absorptivity quickly grows until around 0.025, but with a maximum energy absorption of 70% at all resonant frequencies around $\tan\delta = 0.01$. For high loss values, the absorptivity decays in a quasi-

Table 2. Comparison of the proposed absorber and previously reported triple-band absorbers.

Ref	Physical Size [mm^3] Electrical Size	Resonance Frequencies	Maximum Absorption	Number of Sub-resonators	Covering Band
(Zeng et al., 2018)	$13.8 \times 13.8 \times 1$ $0.202\lambda_0 \times 0.202\lambda_0 \times 0.014\lambda_0$	4.4 GHz, 6.05 GHz, 13.9 GHz	95%, 97%, 97%	2	C, Ku
(Jiang et al., 2016)	$30 \times 30 \times 2$ $0.22\lambda_0 \times 0.22\lambda_0 \times 0.015\lambda_0$	2.29 GHz, 4.28 GHz, 11.71 GHz	98.7%, 99.4%, 99.5%	5	S, C, X
(Ma et al., 2014)	$30 \times 30 \times 1$ $0.616\lambda_0 \times 0.616\lambda_0 \times 0.02\lambda_0$	6.16 GHz, 8.76 GHz, 12.54 GHz	99.87%, 99.98%, 99.99%	3	C, X, Ku
(Deng et al., 2020)	$8 \times 8 \times 0.4$ $0.226\lambda_0 \times 0.226\lambda_0 \times 0.011\lambda_0$	8.5 GHz, 13.5 GHz, 17.0 GHz	99.9%, 99.5%, 99.9%	3	X, Ku
(Xu et al., 2012)	$10.6 \times 10.6 \times 3$ $0.07\lambda_0 \times 0.07\lambda_0 \times 0.02\lambda_0$	2.09 GHz, 6.53 GHz, 10.3 GHz	94%, 92%, 92.3%	3	S, C, X
(Hossain et al., 2022)	$10 \times 10 \times 1.6$ $0.179\lambda_0 \times 0.179\lambda_0 \times 0.028\lambda_0$	5.37 GHz, 10.32 GHz, 12.25 GHz	99.9%, 99.9%, 99.7%	3	C, X, Ku
(Mishra et al., 2017)	$8 \times 8 \times 0.8$ $0.11\lambda_0 \times 0.11\lambda_0 \times 0.011\lambda_0$	4.19 GHz, 9.34 GHz, 11.48 GHz	99.67%, 99.48%, 99.42%	2	C, X
(Singh et al., 2019)	$14 \times 14 \times 0.5$ $0.195\lambda_0 \times 0.195\lambda_0 \times 0.007\lambda_0$	4.19 GHz, 6.64 GHz, 9.95 GHz	97.5%, 96.5%, 98.85%	3	C, X
(Hakim et al., 2023)	$9.5 \times 9.5 \times 1.6$ $0.116\lambda_0 \times 0.116\lambda_0 \times 0.013\lambda_0$	2.5 GHz, 4.9 GHz, 6 GHz	90%, 99%, 97%	2	S, C
(Jain et al., 2021)	$10 \times 10 \times 1.6$ $0.112\lambda_0 \times 0.112\lambda_0 \times 0.018\lambda_0$	3.36 GHz, 3.95 GHz, 10.48 GHz	99.42%, 99.1%, 99.9%	2	S, X
(Divya & Sood, 2021)	$10 \times 10 \times 0.8$ $0.13\lambda_0 \times 0.13\lambda_0 \times 0.01\lambda_0$	3.92 GHz, 5.92 GHz, 9.2 GHz	99.2%, 94.5%, 99.5%	3	S, C, X
(Genikala et al., 2023)	$15.1 \times 15.1 \times 1.6$ $0.121\lambda_0 \times 0.121\lambda_0 \times 0.013\lambda_0$	2.41 GHz, 5.51 GHz, 7.52 GHz	99.5%, 99.3%, 99.9%	3	S, C
This work	$13.24 \times 13.24 \times 2$ $0.35\lambda_0 \times 0.35\lambda_0 \times 0.05\lambda_0$	8.1 GHz, 15.39 GHz, 19.7 GHz	99.43%, 93.45%, 99.02%	1	X, Ku, K

exponential manner, reaching values below 50% at all frequencies for a loss tangent value of 0.4. As it is evident, a higher value of tanδ does not always result in higher absorption, since this value can affect the input impedance of the absorber and, then, most of the incident energy would be reflected.

Figure 11 shows the electric field distribution in the MMA for an electromagnetic wave under normal incidence with an x-directed electric field. At 8.1 GHz, a higher concentration of the electric field can be observed mainly in the formations of the structure along the x-direction. At 15.39 GHz, a strong electric field is observed in the x-directed slits and edges of the circular geometry. Finally, a sharp electric field is also observed at 19.7 GHz, as shown in Fig. 11(c), where the E-field is mostly concentrated in the x-directed slits and diagonal edges of the cell. From the simulated electric field distribution at these three absorption frequencies, one can note a strong electrical coupling between adjacent elements, which indicates the presence of magnetic resonances. Therefore, both the electrical and magnetic resonances contribute to high absorption rates in the proposed structure according to the electric field distribution.

Figure 12 shows the absorption spectrum according to the evolution of the design steps. In all simulations performed in this study, the simulation procedure is the same, where a normally incident EM wave illuminates the structure along the z-axis (see Fig. 1(b)). Considering the unit cell comprising only one slot (D1), it is observed that this simple aperture provides strong resonance at 9.01 GHz with an absorptivity of 91.32% (dashed line). When the unit cell contains three slots (D2), as shown in the inset of Fig. 12, two absorption peaks are noted with absorptivity of 96.21% and 98.56% at the resonant frequencies of 6.53 GHz and 15.41 GHz, respectively. The final structure of the proposed metamaterial absorber is obtained by inserting slots as discussed earlier. The insertion of one more slot along the vertical line in the D2 design (forming a cross-shaped structure) does not change either the number of peaks or the absorption levels, with only a slight shift in frequency in relation to the D2 design. However, the insertion of the slits, as shown in the final design, in addition to ensuring insensitivity to polarization, adds

one more peak, all above 93% absorption. Thus, the enhancement in absorption levels along with a slight frequency shift is due to the mutual coupling effect. In this study, only peaks with absorption higher than 90% were considered.

To provide a comparison among the proposed MTM absorber and the other absorbers previously reported in the literature, Table 2 shows their unit cell size, electrical size, which is calculated at the minimum frequency of absorption, resonance frequencies, maximum absorption, and the number of sub-resonators. One can note that the proposed absorber is relatively thin, which is only 0.05 times the wavelength at the lowest absorption frequency. Furthermore, compared to the three-band MMAs proposed previously, it has only one sub-resonator, unlike the other structures.

5 Conclusion

A triple-band metamaterial absorber has been proposed by using a circle-shaped geometry. By introducing slots into the circular patch, electrical and magnetic resonances are obtained, allowing absorption in three distinct peaks, which are 8.1 GHz, 15.39 GHz, and 19.7 GHz with absorption rates of 99.43%, 93.45%, and 99.02% (99.8%, 99.7%, and 99.8% in measurements), respectively. The absorption mechanism was discussed based on the the single-layer effective medium (SLEM) model and the analysis of surface current and electric field distributions. To verify the absorption performance of the proposed design, a sample of the absorber was fabricated. Both numerical simulation and measurement results show that the proposed metasurface can efficiently absorb EM waves in the three different frequency ranges with an average absorption rate of over 99%. The influence of the dielectric substrate loss level on the absorption responses was investigated. We have shown that a high value of the loss tangent does not necessarily lead to a higher absorption level and that, for the three absorption peaks, the actual design leads to absorption close to unity. **The ultrathin thickness and small size make the structure suitable for applications such as energy harvesting, sensor and RCS reduction.**

References

Agarwal, M., & Meshram, M. K. (2018). Metamaterial-based dual-band microwave absorber with polarization insensitive and wide-angle performance. *AIP Advances*, *8*(9), 095016.

Ängskog, P., Bäckström, M., Samuelsson, C., & Vallhagen, B. K. (2018). Shielding effectiveness and hpm vulnerability of energy-saving windows and window panes. *IEEE Transactions on Electromagnetic Compatibility*, *61*(3), 870–877.

Bhattacharyya, S., Ghosh, S., & Vaibhav Srivastava, K. (2013). Triple band polarization-independent metamaterial absorber with bandwidth enhancement at x-band. *Journal of Applied Physics*, *114*(9), 094514.

Bhattacharyya, S., & Srivastava, K. V. (2014). Triple band polarizationindependent ultra-thin metamaterial absorber using electric field-driven lc resonator. *Journal of Applied Physics*, *115*(6), 064508.

Chaurasiya, D., Ghosh, S., Bhattacharyya, S., & Srivastava, K. V. (2015). An ultra-thin quad-band polarization-insensitive wide-angle metamaterial absorber. *Microwave and Optical technology letters*, *57*(3), 697–702.

Cong, L., Tan, S., Yahiaoui, R., Yan, F., Zhang, W., & Singh, R. (2015). Experimental demonstration of ultrasensitive sensing with terahertz metamaterial absorbers: A comparison with the metasurfaces. *Applied Physics Letters*, *106*(3), 031107.

Deng, G., Lv, K., Sun, H., Yang, J., Yin, Z., Li, Y., ... Li, X. (2020). An ultrathin, triple-band metamaterial absorber with wide-incident-angle stability for conformal applications at x and ku frequency band. *Nanoscale Research Letters*,

15(1), 1–10.

Divya, & Sood, D. (2021). Ultrathin compact triple-band polarization-insensitive metamaterial microwave absorber. In *Mobile radio communications and 5g networks.* Springer.

Faniayeu, I., Asadchy, V., & Fanyaev, I. (2020). Polarization control with helical metasurfaces. *Crystals*, *10*(9), 726.

Ford, K. L., & Chambers, B. (2007). Application of impedance loading to geometric transition radar absorbent material. *IEEE transactions on electromagnetic compatibility*, *49*(2), 339–345.

Gau, J.-R., Burnside, W. D., & Gilreath, M. (1997). Chebyshev multilevel absorber design concept. *IEEE Transactions on Antennas and Propagation*, *45*(8), 1286–1293.

Genikala, S., Ghosh, A., & Roy, B. (2023). Triple band single layer microwave absorber based on closed loop resonator structures with high stability under oblique incidence. *AEU - International Journal of Electronics and Communications*, *64*, 1—9.

Ghosh, S., & Srivastava, K. V. (2017). Polarization-insensitive dual-band switchable absorber with independent switching. *IEEE Antennas and Wireless Propagation Letters*, *16*, 1687–1690.

Hakim, M. L., Islam, M. T., Alam, T., Abdul Rahim, S. K., Bais, B., Islam, M. S., & Soliman, M. S. (2023). Triple-band square split-ring resonator metamaterial absorber design with high effective medium ratio for 5g sub-6 ghz applications. *Nanomaterials*, *13*(2), 222.

Holloway, C. L., Dienstfrey, A., Kuester, E. F., O'Hara, J. F., Azad, A. K., & Taylor, A. J. (2009). A discussion on the interpretation and characterization of metafilms/metasurfaces: The two-dimensional equivalent of metamaterials. *Metamaterials*, *3*(2), 100–112.

Hossain, M. B., Faruque, M. R. I., Islam, M. T., Singh, M., & Jusoh, M. (2022). Triple band microwave metamaterial absorber based on double e-shaped symmetric split ring resonators for emi shielding and stealth applications. *Journal of Materials Research and Technology*, *18*, 1653–1668.

Huang, S., Xie, Z., Chen, W., Lei, J., Wang, F., Liu, K., & Li, L. (2018). Metasurface with multi-sized structure for multi-band coherent perfect absorption. *Optics express*, *26*(6), 7066–7078.

Islam, M. R., Islam, M. T., Moniruzzaman, M., Samsuzzaman, M., & Arshad, H. (2021). Penta band single negative meta-atom absorber designed on square enclosed star-shaped modified split ring resonator for s-, c-, x-and ku-bands microwave applications. *Scientific Reports*, *11*(1), 1–22.

Jain, P., Singh, A. K., Pandey, J. K., Bansal, S., Sardana, N., Kumar, S., ... Singh, A. K. (2021). An ultrathin compact polarization-sensitive triple-band microwave metamaterial absorber. *Journal of Electronic Materials*, *50*, 1506—1513.

Jiang, H., Xue, Z., Li, W., & Ren, W. (2016). Multiband polarisation insensitive metamaterial absorber based on circular fractal structure. *IET Microwaves, Antennas & Propagation*, *10*(11), 1141–1145.

Karamirad, M., Ghobadi, C., & Nourinia, J. (2020). Metasurfaces for wideband and efficient polarization rotation. *IEEE Transactions on Antennas and Propagation*, *69*(3), 1799–1804.

Knott, E. F., Schaeffer, J. F., & Tulley, M. T. (2004). *Radar cross section.* SciTech Publishing.

Landy, N. I., Sajuyigbe, S., Mock, J. J., Smith, D. R., & Padilla, W. J. (2008). Perfect metamaterial absorber. *Physical review letters*, *100*(20), 207402.

Li, H., Yuan, L. H., Zhou, B., Shen, X. P., Cheng, Q., & Cui, T. J. (2011). Ultrathin multiband gigahertz metamaterial absorbers. *Journal of Applied Physics*, *110*(1), 014909.

Li, S. J., Li, Y. B., Li, R. Q., Cheng, Q., & Cui, T. J. (2020). Digital-coding-feeding metasurfaces for differently polarized wave emission, orbit angular momentum generation, and scattering manipulation. *Advanced Photonics Research*, *1*(1), 2000012.

Lim, D., & Lim, S. (2019). Ultrawideband electromagnetic absorber using sandwiched broadband metasurfaces. *IEEE Antennas and Wireless Propagation Letters*, *18*(9), 1887–1891.

Luo, H., Cheng, Y. Z., & Gong, R. Z. (2011). Numerical study of metamaterial absorber and extending absorbance bandwidth based on multi-square patches. *The European Physical Journal B*, *81*, 387–392.

Ma, B., Liu, S., Bian, B., Kong, X., Zhang, H., Mao, Z., & Wang, B. (2014). Novel three-band microwave metamaterial absorber. *Journal of Electromagnetic Waves and Applications*, *28*(12), 1478–1486.

Mishra, N., Choudhary, D. K., Chowdhury, R., Kumari, K., & Chaudhary, R. K. (2017). An investigation on compact ultra-thin triple band polarization independent metamaterial absorber for microwave frequency applications. *IEEE Access*, *5*, 4370–4376.

Padooru, Y. R., Yakovlev, A. B., Chen, P.-Y., & Alu, A. (2012). Line-source excitation of realistic conformal metasurface cloaks. *Journal of Applied Physics*, *112*(10), 104902.

Pan, W., Shen, T., Ma, Y., Zhang, Z., Yang, H., Wang, X., ... Yang, L. (2021). Dual-band and polarization-independent metamaterial terahertz narrowband absorber. *Applied Optics*, *60*(8), 2235–2241.

Pang, Y., Li, Y., Qu, B., Yan, M., Wang, J., Qu, S., & Xu, Z. (2020). Wideband rcs reduction metasurface with a transmission window. *IEEE Transactions on Antennas and Propagation*, *68*(10), 7079–7087.

Sarkhel, A., & Chaudhuri, S. R. B. (2017). Compact quad-band polarization-insensitive ultrathin metamaterial absorber with wide angle stability. *IEEE Antennas and Wireless Propagation Letters*, *16*, 3240–3244.

Singh, A. K., Abegaonkar, M. P., & Koul, S. K. (2019). Dual- and triple-band polarization insensitive ultrathin conformal metamaterial absorbers with wide angular stability. *IEEE Transactions on Electromagnetic Compatibility*, *61*(3), 878–886.

Tao, H., Landy, N. I., Bingham, C. M., Zhang, X., Averitt, R. D., & Padilla, W. J. (2008). A metamaterial absorber for the terahertz regime: design, fabrication and characterization. *Optics express*, *16*(10), 7181–7188.

Wang, B.-X., Tang, C., Niu, Q., He, Y., & Chen, R. (2019). A broadband terahertz metamaterial absorber enabled by the simple design of a rectangular-shaped resonator with an elongated slot. *Nanoscale Advances*, *1*(9), 3621–3625.

Wang, S., Hou, B., & Chan, C. T. (2019). Broadband microwave absorption by logarithmic spiral metasurface. *Scientific reports*, *9*(1), 1–7.

Wang, X., Wang, Q., Dong, G., Hao, Y., Lei, M., & Bi, K. (2017). Multi-band terahertz metasurface absorber. *Modern Physics Letters B*, *31*(36), 1750354.

Watts, C. M., Liu, X., & Padilla, W. J. (2012). Metamaterial electromagnetic wave absorbers. *Advanced materials*, *24*(23), OP98–OP120.

Xu, H.-X., Wang, G.-M., Qi, M.-Q., Liang, J.-G., Gong, J.-Q., & Xu, Z.-M. (2012). Triple-band polarization-insensitive wide-angle ultra-miniature metamaterial transmission line absorber. *Physical Review B*, *86*(20), 205104.

Yang, D., & Xia, Y. (2020). Experimental verification of multi-band metamaterial absorber with double structured layers. *Materials Research Express*, *7*(3), 035801.

Zadeh, A. K., & Karlsson, A. (2009). Capacitive circuit method for fast and efficient design of wideband radar absorbers. *IEEE Transactions on Antennas and Propagation*, *57*(8), 2307–2314.

Zeng, X., Zhang, L., Wan, G., Gao, M., & Hu, B. (2018, Dec.). An ultra-thin triple-

band metamaterial absorber with equivalent circuit analysis. In *Proc. of eucap.* London.

Zhao, G., Bi, S., & Cui, Y. (2019). Study on the characteristics of a v-shaped metamaterial absorber and its application. *AIP Advances*, *9*(7), 075016.